






RESEARCH ARTICLE | JANUARY 28 2019

Comparative study on the use of novel heteroleptic cyclopentadienyl-based zirconium precursors with H₂O and O₃ for atomic layer deposition of ZrO₂

Special Collection: [2019 Special Collection on Atomic Layer Deposition \(ALD\)](#)

Sanni Seppälä ; Marko Vehkamäki; Kenichiro Mizohata; Wontae Noh; Jyrki Räisänen; Mikko Ritala ; Markku Leskelä 



J. Vac. Sci. Technol. A 37, 020912 (2019)

<https://doi.org/10.1116/1.5079539>



Articles You May Be Interested In

Role of a cyclopentadienyl ligand in a heteroleptic alkoxide precursor in atomic layer deposition

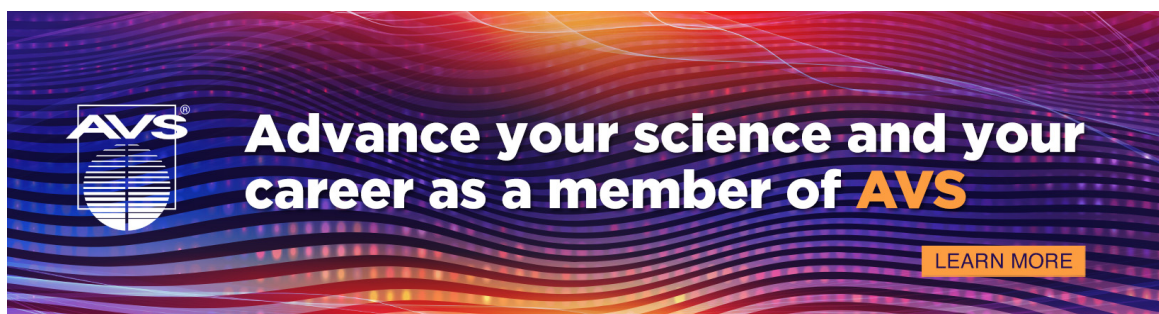
J. Chem. Phys. (January 2024)

Recent trends in thermal atomic layer deposition chemistry

J. Vac. Sci. Technol. A (March 2025)

In situ reaction mechanism studies on the Ti(NMe₂)₂(OⁱPr)₂-D₂O and Ti(OⁱPr)₃[MeC(NⁱPr)₂]-D₂O atomic layer deposition processes

J. Vac. Sci. Technol. A (December 2013)



Advance your science and your career as a member of AVS

[LEARN MORE](#)

Comparative study on the use of novel heteroleptic cyclopentadienyl-based zirconium precursors with H₂O and O₃ for atomic layer deposition of ZrO₂

Sanni Seppälä,^{1,a)} Marko Vehkamäki,¹ Kenichiro Mizohata,² Wontae Noh,³
 Jyrki Räisänen,² Mikko Ritala,¹ and Markku Leskelä¹

¹Department of Chemistry, University of Helsinki, P.O. Box 55, FI-00014 Helsinki, Finland

²Division of Materials Physics, Department of Physics, University of Helsinki, P.O. Box 43, FI-00014 Helsinki, Finland

³Air Liquide Laboratories Korea, Yonsei Engineering Research Park, 50 Yonsei-ro, Seodaemun-gu, Seoul 03722, South Korea

(Received 31 October 2018; accepted 3 January 2019; published 28 January 2019)

Three heteroleptic Zr precursors were studied for atomic layer deposition (ALD) of ZrO₂. Films were deposited from Zr(Cp)(^tBuDAD)(OⁱPr), Zr(MeCp)(TMEA), and Zr(Me₅Cp)(TEA) with either water or ozone as the oxygen source {^tBuDAD = N,N-bis(tertbutyl)ethene-1,2-diaminato, TMEA = tris[2-(methylamino)ethyl]amine, TEA = triethanolamine}. Self-limiting film growth was confirmed for the Zr(Cp)(^tBuDAD)(OⁱPr)/O₃ process at 250 °C and for the Zr(Me₅Cp)(TEA)/O₃ process at 375 °C, which is among the highest temperatures for advanced heteroleptic precursors. Excellent film purity with C, H, and N levels below the detection limit of the elastic recoil detection analysis was obtained with ozone as the oxygen source. All the studied processes showed the same trend that at low deposition temperatures films were tetragonal ZrO₂ and at higher temperatures mixtures of tetragonal and monoclinic ZrO₂. With water, the monoclinic phase appeared at higher temperatures than with ozone. In addition to the deposition temperature, the film thickness affected the phase; thinner films favored the tetragonal phase and monoclinic peaks were more clearly seen in thicker films. The high thermal stability and excellent film purity show that from the three studied Zr precursors, Zr(Me₅Cp)(TEA) is a noteworthy precursor candidate for ALD of ZrO₂. *Published by the AVS.* <https://doi.org/10.1116/1.5079539>

I. INTRODUCTION

Zirconium dioxide is a very interesting material as an dielectric for micro-electronics, and it has been studied extensively particularly for memory applications.^{1,2} Other applications include electrolytes and interlayers for solid oxide fuel cells (SOFCs),^{3,4} and lately ZrO₂ films have also been studied for antibacterial purposes.⁵ Zirconium dioxide has a bandgap of 5.8 eV, and a suitable band offset of 1.4 eV to Si.⁶ The relative permittivity of ZrO₂ in the bulk form is between 20 (monoclinic ZrO₂) and 47 (tetragonal ZrO₂). The monoclinic phase is stable at room temperature and the change from the monoclinic phase to the most desired high permittivity tetragonal phase occurs above 1100 °C.⁷ However, in thin films, tetragonal, cubic, and orthorhombic ZrO₂ have been identified.^{8–10} The effect of the surface energy is enhanced in thin films, making the appearance of high pressure and temperature phases possible.

Atomic layer deposition (ALD) is the method of choice to produce highly conformal and uniform thin films, especially for the microelectronic applications.¹¹ The first ZrO₂ process for ALD was ZrCl₄/H₂O.^{12–15} Since then, various Zr precursors have been studied extensively, including amidinates, β-diketonates, and alkylamides.^{9,16,17} Unfortunately, all these have drawbacks regarding either growth rate or thermal stability.

Heteroleptic precursors, i.e., precursors with more than one type of ligands in the metal complex, have been widely studied for Zr. Possible benefits include better thermal stability, volatility, and reactivity compared to the homoleptic counterparts.¹⁸ However, it is not always easy to predict the properties of the heteroleptic compounds and sometimes the result can be a combination of the undesirable properties of the ligands. Thus, it is important to study different heteroleptic compounds to understand the benefits they can offer compared to the traditional ALD precursors.

Advanced heteroleptic zirconium precursors applied in ALD most often have cyclopentadienyl (Cp) ring as one of the ligands. Cyclopentadienyls are good electron donors and form stable bonds with metals, which ensure good thermal stability of the compounds.¹⁹ Also, the properties of the Cp ligands can easily be tuned by varying the number and composition of the substitutes on the ring. Examples of heteroleptic precursors with Cp ligands are RCpZr(NMe₂)₃ (R = H, ethyl or methyl),²⁰ RCp₂ZrMe₂ (R = H or methyl),²¹ and MeCpZrCHT (CHT = cycloheptatrienyl).²² Many of the heteroleptic precursors have been reported to exhibit self-limiting growth at 300 °C, including the CpZr(NMe₂)₃ that is widely used in industry.²³ RCp₂ZrMe₂ has a higher thermal stability of 350 °C but the as-deposited films consist of the low permittivity monoclinic ZrO₂.

In this work, three heteroleptic zirconium precursors were studied as Zr sources in the atomic layer deposition of ZrO₂. These compounds were cyclopentadienyl N,N-bis(tertbutyl)ethene-1,2-diaminato isopropylalkoxo zirconium Zr(Cp)

Note: This paper is part of the 2019 special collection on Atomic Layer Deposition (ALD).

^{a)}Electronic mail: sanni.seppala@helsinki.fi

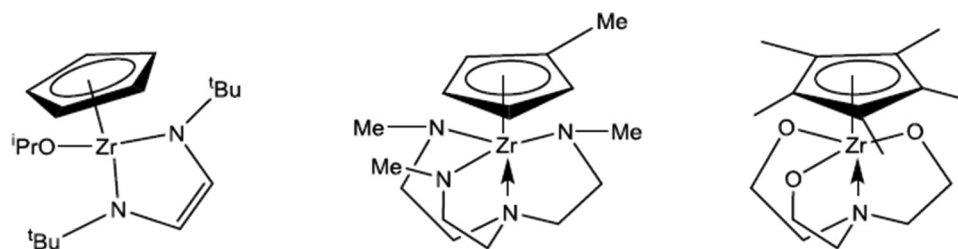


FIG. 1. Schematic structures of the zirconium precursors $\text{Zr}(\text{Cp})(\text{tBuDAD})(\text{OiPr})$, $\text{Zr}(\text{MeCp})(\text{TMEA})$, and $\text{Zr}(\text{Me}_5\text{Cp})(\text{TEA})$.

$(\text{tBuDAD})(\text{OiPr})$, methylcyclopentadienyl tris[2-(methylamino)ethyl]amine zirconium $\text{Zr}(\text{MeCp})(\text{TMEA})$, and pentamethylcyclopentadienyl triethanolamine zirconium $\text{Zr}(\text{Me}_5\text{Cp})(\text{TEA})$ (Fig. 1). All three precursors have a Cp ring as one of the ligands but the number of substituents in the ring varies. tBuDAD , TMEA , and TEA ligands were used to attain better thermal stability compared to the state-of-the-art heteroleptic precursors and at the same time to retain reasonable volatility for the precursors.

II. EXPERIMENT

A. Precursor characterization

Thermogravimetric analyses (TGAs) and precursor vapor pressure studies were carried out in a Mettler Toledo TGA/DSC 1 STARe System. Measurements were done under nitrogen atmosphere with a nitrogen flow of 220 sccm/min at atmospheric pressure. $\text{Zr}(\text{Me}_5\text{Cp})(\text{TEA})$ was also studied under vacuum with a pressure of 20 Torr. A heating program of 10 °C/min was used in all the measurements. Vapor pressures were estimated by using evaporation rate at each temperature.

B. Film deposition

Films were deposited in a hot-wall cross-flow F-120 ALD reactor (ASM Microchemistry) from $\text{Zr}(\text{Cp})(\text{tBuDAD})(\text{OiPr})$, $\text{Zr}(\text{MeCp})(\text{TMEA})$, and $\text{Zr}(\text{Me}_5\text{Cp})(\text{TEA})$ precursor (all from Air Liquide) with either water or ozone as the oxygen source. The Zr precursors were solid at room temperature, but $\text{Zr}(\text{Cp})(\text{tBuDAD})(\text{OiPr})$ and $\text{Zr}(\text{MeCp})(\text{TMEA})$ melted in the reactor at their source temperature. The evaporation temperatures for the precursors were 65 °C for $\text{Zr}(\text{Cp})(\text{tBuDAD})(\text{OiPr})$, 115 °C for $\text{Zr}(\text{Me}_5\text{Cp})(\text{TEA})$, and 120 °C for $\text{Zr}(\text{MeCp})(\text{TMEA})$. The deposition temperatures were varied in the range of 200–425 °C. The reactor pressure was ~5 mbar. Water was kept in a container at room temperature outside the reactor and the vapor flow was controlled by a needle valve. Ozone with a concentration of 100 g/m³ was generated from O₂ (AGA 99.999%) in an ozone generator (Wedeco Modular 4 HC). Nitrogen (AGA 99.999% H₂O ≤ 3 ppm, O₂ ≤ 3 ppm) was used as the carrier and purging gas. Si(100) wafers cut to 5 × 5 cm² pieces were used as substrates. Native oxide was not removed prior to deposition. For electrical measurements, films were deposited on Pt substrates.

C. Film characterization

Film thicknesses were measured with x-ray reflectivity using a Rigaku SmartLab x-ray diffractometer. Film densities

were obtained by fitting the XRR data. Crystallinity and phase of the films were determined by grazing incidence x-ray diffraction (GIXRD) with a PANalytical X'Pert Pro MPD diffractometer.

TEM specimens were prepared with the focused ion beam (FIB) lift-out method, with an FEI Quanta 3D 200i DualBeam instrument. Bright-field TEM images were collected with a 200 kV Tecnai F20 transmission electron microscope.

Film compositions were examined with time-of-flight elastic recoil detection analysis (TOF-ERDA) at a detection angle of 40° by 40 MeV ⁷⁹Br⁷⁺ ions obtained from a 5 MV tandem accelerator EGP-10-II.

For the electrical measurements, metal-insulator-metal (MIM) plate capacitors with Pt/ZrO₂/Al structures were made. ZrO₂ films were deposited on Pt evaporated on Si wafer. Aluminum dots with an area of 0.204 mm² were e-beam evaporated through a shadow mask on the top of the ZrO₂ films. The dot diameter used for calculating the area was obtained from SEM images. The Pt electrode thickness was 40 nm, and the Al dot thicknesses were approximately 90 nm. There were vacuum breaks between all depositions. Current–voltage (I–V) characteristics were measured with a Keithley 2400 source meter with a step size of 0.2 V/step. The capacitance values were measured with a HP4284A LCR meter with a frequency of 10 kHz. Relative permittivities were calculated from the mean capacitances.

III. RESULTS AND DISCUSSION

A. Precursor properties

The TG curves of the three precursors are depicted in Fig. 2(a). $\text{Zr}(\text{Cp})(\text{tBuDAD})(\text{OiPr})$ and $\text{Zr}(\text{MeCp})(\text{TMEA})$ showed a single step weight loss in atmospheric pressure. The residue for the $\text{Zr}(\text{Cp})(\text{tBuDAD})(\text{OiPr})$ precursor was very low, below 2%, indicating evaporation without decomposition. For the $\text{Zr}(\text{MeCp})(\text{TMEA})$ precursor, the residue was around 15% which means that the precursor is also decomposing.

$\text{Zr}(\text{Me}_5\text{Cp})(\text{TEA})$ showed a two-step weight loss process with a residue of 65% after the first step and 30% at the end of the measurement (500 °C) at atmospheric pressure. Because of the high residues, also a measurement under vacuum was conducted. The results in vacuum were clearly better than in atmospheric pressure as the residue after the first step at 230 °C was 15%. Despite the decomposition seen in the TG analysis, in the ALD experiments, the first signs of precursor decomposition were seen only at 400 °C. Differences in the decomposition temperature between TG analysis and ALD deposition

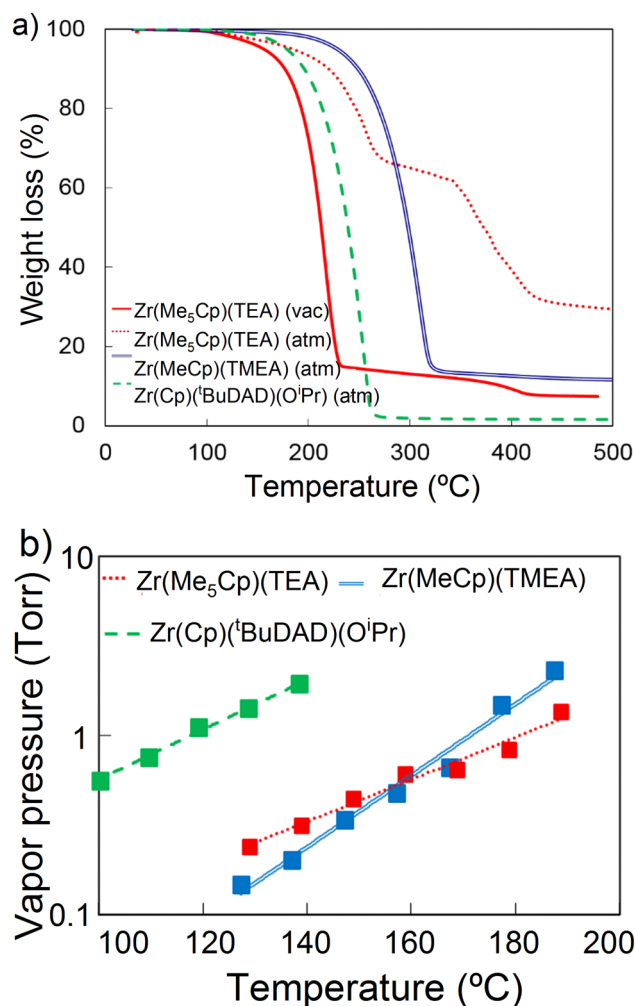


FIG. 2. (a) Thermogravimetric analysis and (b) vapor pressures of the Zr precursors.

experiments have previously been reported, for example, in ALD of CoO from CoCl₂(TMEDA) (TMEDA = *N,N,N',N'*-tetramethylethylenediamine)²⁴ and the probable cause for this comes from the differences in interactions in the gas phase and on the surface during the ALD process as compared to the interactions in the condensed phase in TG.

Vapor pressure studies of the precursors were in line with the TG results and showed that Zr(Cp)(^tBuDAD)(OⁱPr) is substantially more volatile than the Zr(MeCp)(TMEA) and Zr(Me₅Cp)(TEA) precursors [Fig. 2(b)]. Based on the vapor pressure, the evaporation temperatures for the ALD experiments were chosen to be 65 °C for Zr(Cp)(^tBuDAD)(OⁱPr) and 120 °C for Zr(MeCp)(TMEA). Sublimation temperature of 115 °C was chosen for the Zr(Me₅Cp)(TEA) precursor.

B. Film deposition

The reactivities of the Zr precursors especially toward water varied largely [Fig. 3(a)]. Zr(Me₅Cp)(TEA) did not react with water below 400 °C and at 400 °C, the growth rate was very low, 0.1 Å/cycle.

With the Zr(MeCp)(TMEA)/H₂O process, films were deposited at 200–375 °C. Almost constant growth rate around

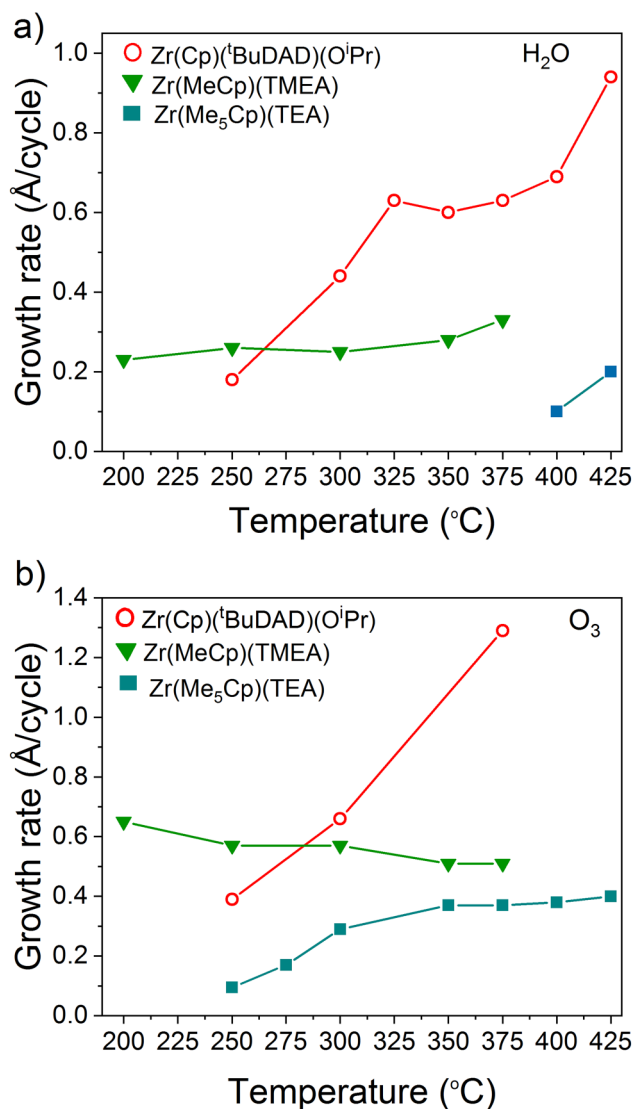


FIG. 3. (a) Film growth rates at different temperatures with (a) water and (b) ozone as the oxygen source. Pulse times for Zr precursors, H₂O and O₃ were 1.0 s and purge times for all pulses 1.5 s.

0.3 Å/cycle was obtained at 250–350 °C. Slight increase in the growth rate was observed at 375 °C. With the Zr(Cp)(^tBuDAD)(OⁱPr)/H₂O process, films were deposited at 250–425 °C. A temperature range with a constant growth rate of around 0.65 Å/cycle was seen from 325 to 400 °C [Fig. 3(a)].

All three precursors had higher growth rates with ozone than with water [Fig. 3(b)]. Zr(Me₅Cp)(TEA)/O₃ had a constant growth rate of 0.4 Å/cycle at 350–400 °C. The growth rate slightly increased at 425 °C because of the precursor decomposition. This decomposition was clearly observed from the appearance of some film deposits in the hot end of the source tube and it was not visible at lower deposition temperatures. The rather slow growth rates with Zr(Me₅Cp)(TEA) are probably caused by the bulky ligands that shield the Zr atoms and prevent reactions. TEA is also a chelating ligand with three oxygen donor atoms that are expected to bond stronger to Zr than the nitrogen donors in TMEA and ^tBuDAD [Zr–O bond strength is ~760 kJ/mol and

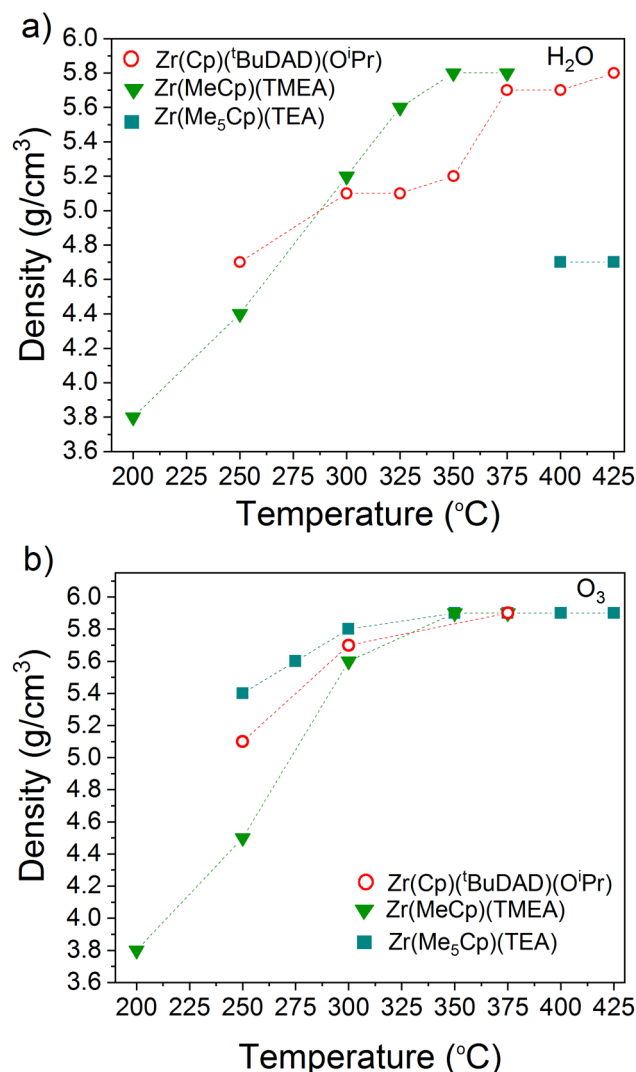


FIG. 4. Film densities at different deposition temperatures with (a) water and (b) ozone as the oxygen source.

Zr-N ~ 560 kJ/mol (Ref. 25)]. The advantage of the Zr(Me₅Cp)(TEA) precursor is its excellent thermal stability compared to the other two precursors.

With the Zr(MeCp)(TMEA)/O₃ process, the growth rate decreased with increasing temperature from 0.65 Å/cycle at 200 °C to 0.50 Å/cycle at 375 °C. Zr(Cp)(tBuDAD)(OᶦPr) with O₃ showed the opposite behavior as the growth rates increased from 0.40 Å/cycle at 250 °C to 1.3 Å/cycle at 375 °C.

The deposition temperature affected the film density as depicted in Fig. 4. The bulk density of ZrO₂ is around 6 g/cm³ depending on the phase. With Zr(MeCp)(TMEA) and Zr(Cp)(tBuDAD)(OᶦPr), a considerable increase in the density was seen with increasing deposition temperature regardless of the oxygen source. With water, the film densities ranged from 5.7 to 5.9 g/cm³ at the highest deposition temperatures, whereas at 250 °C the density decreased to 4.4 g/cm³ for Zr(MeCp)(TMEA) (3.8 g/cm³ at 200 °C) and 4.7 g/cm³ for Zr(Cp)(tBuDAD)(OᶦPr) [Fig. 4(a)]. With ozone, slightly higher densities compared to water processes were observed at 250 °C. Because of the changes in the film density, the amount of

material deposited, for example, in the Zr(MeCp)(TMEA) processes is much higher at 350 °C (1.47 and 0.79 Zr atoms/nm² cycle with O₃ and H₂O) and 375 °C (1.47 and 0.93 Zr atoms/nm² cycle with O₃ and H₂O) compared to 250 °C (1.30 and 0.55 Zr atoms/nm² cycle with O₃ and H₂O) even though the growth rates are close to each other. Likewise, taking the density increase into account, the increase of the growth rate with increasing temperature in the Zr(Cp)(tBuDAD)(OᶦPr)/O₃ process gets even stronger: 1.0 Zr atoms/nm² cycle at 250 °C, 1.8 Zr atoms/nm² cycle at 300 °C, and 3.9 atoms/nm² cycle at 375 °C.

Films deposited with Zr(Me₅Cp)(TEA) and ozone showed only a small decrease in density from 5.9 to 5.4 g/cm³ while decreasing the deposition temperature [Fig. 4(b)]. The thickness of the films did not affect the density: films with thicknesses around 10 nm showed densities similar to 40 nm thick films at 300–375 °C. With water, density was very low (4.7 g/cm³) compared to the ozone process despite the high deposition temperatures of 400 and 425 °C [Fig. 4(a)]. The film thicknesses were similar in both processes. The low density appears to be due to the low reactivity of the Zr(Me₅Cp)(TEA) precursor with water which is seen in the low growth rate [Fig. 3(a)] and high impurity concentrations (Table I) in the films. Because of the low densities and very low growth rates, only a few films with the Zr(Me₅Cp)(TEA)/H₂O process were deposited.

The effect of the Zr precursor pulse length on the growth rate was studied to reveal the true, self-limiting ALD-type growth processes. Self-limiting growth mode was confirmed for the Zr(Me₅Cp)(TEA)/O₃ process at 300, 350 (not shown), and 375 °C (Fig. 5). The growth rate was 0.3 Å/cycle at 300 °C and 0.4 Å/cycle at 350 and 375 °C. At 400 °C, the growth rate increased slightly with increasing pulse length from 0.38 Å/cycle at 1.0 s pulse length to 0.46 Å/cycle at 3.5 s Zr precursor pulse. This result demonstrates that the thermal stability of the Zr(Me₅Cp)(TEA) precursor is one of the highest among zirconium precursors and clearly higher than the thermal stability of the industrially dominant CpZr(NMe₂)₃ precursor which saturates at 300 °C.²⁰ Despite the very strong temperature dependence, self-limiting growth was also observed in the Zr(Cp)(tBuDAD)(OᶦPr)/O₃ process at 250 °C (0.5 Å/cycle) but not at higher deposition temperatures. However, at this low deposition temperature, the film density was somewhat lower than the bulk value of ZrO₂. Zr(MeCp)(TMEA) did not show saturation of the growth with ozone and none of the Zr precursors saturated when water was used as the oxygen source. The saturation studies for the ozone processes are shown in Fig. 5.

C. Film characterization

All the three studied precursors showed similar trends regarding film crystallinity: The films were crystalline ZrO₂, and the phase was either tetragonal ZrO₂ (ICDD 50-1089) or a mixture of tetragonal and monoclinic (ICDD 37-1484) ZrO₂ depending on the growth temperature and oxygen source. At low deposition temperatures, only tetragonal phase was seen. With water, the temperature at which the monoclinic phase appeared was higher than with ozone. The

TABLE I. TOF-ERDA results from selected samples.

Zr source	O source	T _{dep} (°C)	Zr (at. %)	O (at. %)	Zr:O ratio	H (at. %)	C (at. %)	N (at. %)
Zr(Me ₅ Cp)(TEA)	O ₃	375	32.1	67.9	0.47	N.D.	N.D.	N.D.
		300	32.5	67.3	0.48	N.D.	0.3	N.D.
Zr(Cp)(^t BuDAD)(O ⁱ Pr)	H ₂ O	425	29.3	59.3	0.49	3.5	6.5	1.3
		375	32.0	67.2	0.48	0.4	0.3	0.1
		300	31.3	67.7	0.46	0.4	0.5	0.1
	O ₃	250	30.1	67.2	0.45	1.0	1.4	0.2
		375	31.7	65.0	0.49	0.4	2.4	0.5
Zr(MeCp)(TMEA)	H ₂ O	300	31.0	65.4	0.47	0.8	2.5	0.4
		375	32.2	67.0	0.48	0.5	0.1	0.1
		300	29.7	64.8	0.46	4.1	0.8	0.4
	O ₃	375	31.4	64.3	0.49	2.2	1.7	0.4
		300	28.8	59.0	0.49	8.8	2.6	0.7

first small peaks from the monoclinic phase were visible at 300 °C with all Zr precursors when ozone was used as the oxygen source. With water, monoclinic peaks were first seen at 400 °C with the Zr(Cp)(^tBuDAD)(OⁱPr) and at 350 °C with the Zr(MeCp)(TMEA) precursor, whereas only tetragonal phase was seen with the Zr(Me₅Cp)(TEA) precursor (at 400 and 425 °C). The intensity of the monoclinic peaks increased with increasing temperature. The effect of the deposition temperature on the crystalline phase of the films is exemplified in Fig. 6 by Zr(Me₅Cp)(TEA)/O₃ and Zr(MeCp)(TMEA)/H₂O processes.

In addition to the deposition temperature, the film thickness affected the phase composition. It has been reported before that in ALD of ZrO₂ very thin films favor the tetragonal phase and with increasing film thickness the intensity of the monoclinic peaks increases.²⁶ The stabilization of the tetragonal phase in thin films has been attributed to the lower

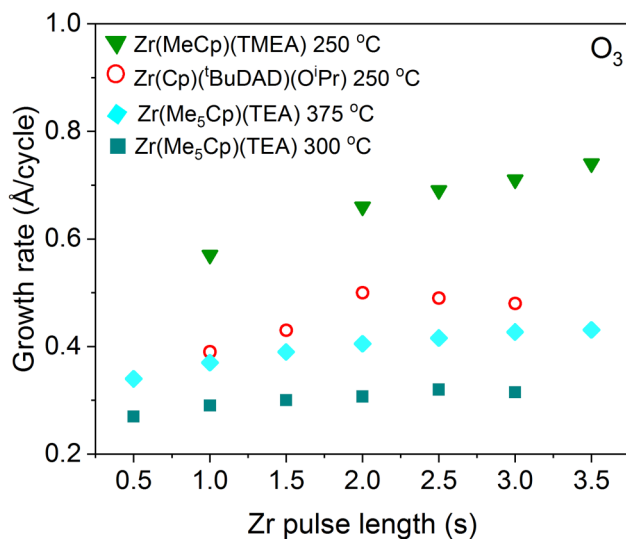


FIG. 5. Film growth rates as a function of Zr precursor pulse length with ozone as the oxygen source. The pulsing sequence was x slx + 0.5 sl1.0 sl1.5 s for Zr pulse/purge/O₃ pulse/purge.

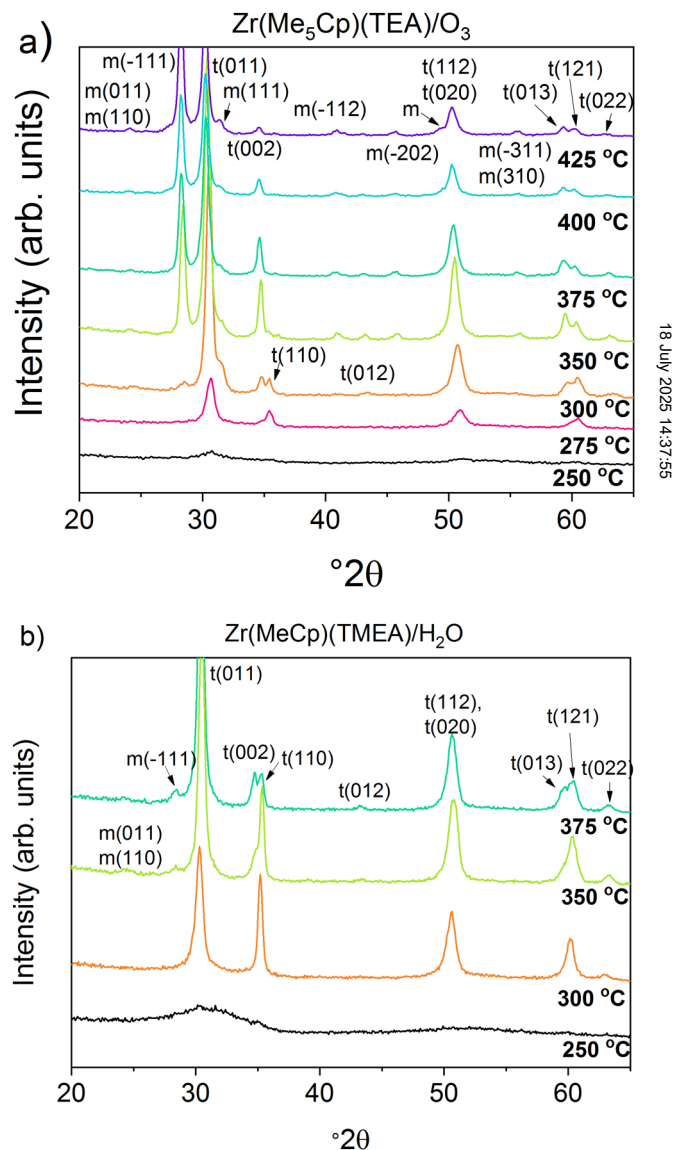


FIG. 6. X-ray diffractograms of the films deposited with (a) Zr(Me₅Cp)(TEA)/O₃ at 250–425 °C and (b) Zr(MeCp)(TMEA)/H₂O process at 250–375 °C. Film thicknesses were in (a) 30–40 nm and in (b) 50 nm except at 375 °C 43 nm.

surface-free energy of the tetragonal phase compared to the monoclinic phase, which is more prominent in nanometer size.²⁷ With all three Zr precursors, thicker films could be deposited with water than with ozone without the monoclinic phase visible in the diffractograms. For example, films with thicknesses between 9 and 70 nm deposited with $\text{Zr}(\text{Cp})(^i\text{BuDAD})(\text{O}^i\text{Pr})/\text{H}_2\text{O}$ at 375 °C were all tetragonal ZrO_2 [Fig. 7(a)]. With the $\text{Zr}(\text{MeCp})(\text{TMEA})/\text{H}_2\text{O}$ process at 350 °C, the first small monoclinic peaks were seen with a film thickness of 50 nm. With ozone, only very thin films were tetragonal: with the $\text{Zr}(\text{MeCp})(\text{TMEA})$ at 350 °C, only the tetragonal phase was detected for a 4 nm thick film, but monoclinic peaks were visible in a 9 nm thick film. For $\text{Zr}(\text{Me}_5\text{Cp})(\text{TEA})/\text{O}_3$ process at 300 °C, 12 nm thick film was tetragonal ZrO_2 but monoclinic peaks could be seen in a 29 nm thick film [Fig. 7(b)]. At 375 °C, a small peak

assigned to the monoclinic phase was visible already in the diffractogram of a 10 nm thick film meaning that the deposition temperature seems to have a stronger impact on the phase composition than the film thickness.

Impurities and film compositions were studied with TOF-ERDA. The results are collected in Table I. In general, the films deposited with ozone had lower impurity contents than the films deposited with water. This kind of trend has been seen previously in oxide ALD depositions.¹⁰ The high purity is attributed to the more efficient removal of the ligands by combustion with ozone than by hydrolysis reactions with water.²⁸ Exceptionally pure films were obtained with the $\text{Zr}(\text{Me}_5\text{Cp})(\text{TEA})/\text{O}_3$ process at 300–375 °C where the carbon, hydrogen, and nitrogen content were below or slightly over the detection limit of TOF-ERDA. In this precursor, Zr is already attached to three oxygen atoms which may explain the high purity. The films deposited with $\text{Zr}(\text{MeCp})(\text{TMEA})$, which did not show saturation of the growth rate (Fig. 5), had higher impurity levels than the others, especially at low deposition temperatures where the hydrogen levels with both water and ozone were considerable.

Capacitor structures were constructed to compare the electrical properties of the different ZrO_2 processes. ZrO_2 films

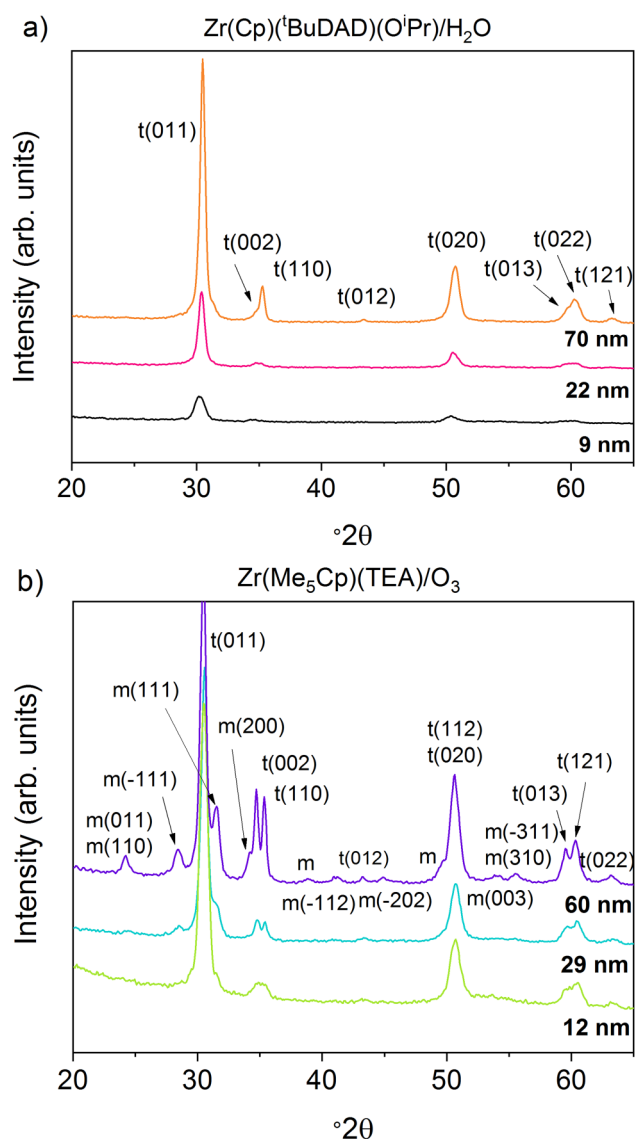


Fig. 7. X-ray diffractograms of films with different thicknesses deposited with (a) $\text{Zr}(\text{Cp})(^i\text{BuDAD})(\text{O}^i\text{Pr})/\text{H}_2\text{O}$ process at 375 °C and (b) $\text{Zr}(\text{Me}_5\text{Cp})(\text{TEA})/\text{O}_3$ process at 300 °C.

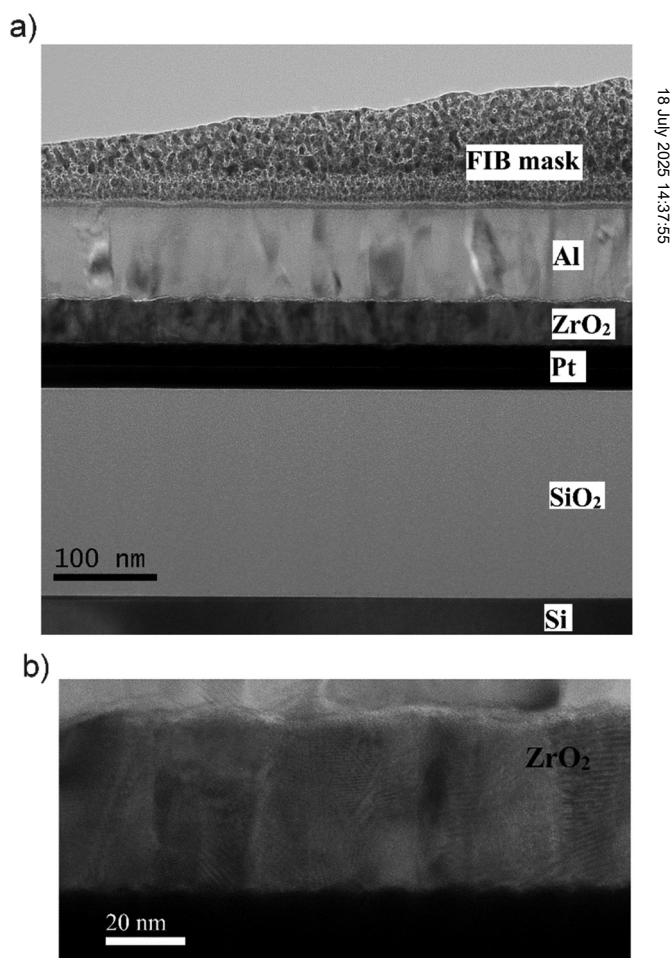


Fig. 8. (a) TEM image of the MIM stack and (b) a close-up of the ZrO_2 film. ZrO_2 was deposited with the $\text{Zr}(\text{Me}_5\text{Cp})(\text{TEA})/\text{O}_3$ process at 300 °C.

TABLE II. Relative permittivities and leakage current densities at 1 MV/cm for different ZrO₂ processes.

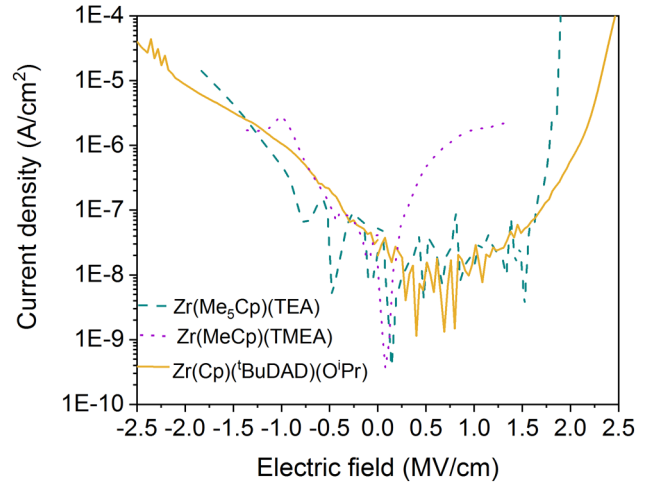
Zr source	O source	T _{dep} (°C)	Film thickness (nm)	ε _r	Leakage current density at 1 MV/cm (A/cm ²)
Zr(Me ₅ Cp)(TEA)	O ₃	375	45	24	5 · 10 ⁻⁸
		350	44	28	3 · 10 ⁻⁸
		300	42	29	2 · 10 ⁻⁸
Zr(Cp)(ⁱ BuDAD)(O ⁱ Pr)	O ₃	300	53	24	2 · 10 ⁻⁸
Zr(MeCp)(TMEA)	H ₂ O	300	42	23	1 · 10 ⁻⁵
	O ₃	300	51	23	2 · 10 ⁻⁶
	H ₂ O	300	62	23	5 · 10 ⁻⁷

for the capacitors were deposited at 300 °C with all processes. For Zr(Me₅Cp)(TEA)/O₃ process, also capacitors with ZrO₂ films deposited at 350 and 375 °C were studied. TEM images of the stack structure are depicted in Fig. 8. Relative permittivities ε_r of the films were calculated from the capacitances using the equation for a parallel plate capacitor [Eq. (1)]:

$$C = \epsilon_0 \epsilon_r \frac{A}{d}, \quad (1)$$

where C is the capacitance, ϵ_0 is the permittivity of the vacuum, A is the area of the capacitor, and d is the thickness of the ZrO₂ layer.

The permittivity values for the ZrO₂ films deposited at 300 °C with different deposition processes ranged from 23 to 29. The highest permittivity was calculated for the film deposited with the Zr(Me₅Cp)(TEA)/O₃. TEM image showed that the lateral grain size in this film is 20–30 nm [Fig. 8(b)]. The permittivities for the other processes remained clearly lower, being 23 or 24 (Table II). The

FIG. 9. Leakage current density curves of the ZrO₂ films deposited with O₃ at 300 °C. The polarity of the electric field indicates the potential applied to the top electrode.

permittivities of the films deposited at 350 and 375 °C with the Zr(Me₅Cp)(TEA)/O₃ process were lower than at 300 °C, probably because of the increasing amount of monoclinic phase in the films. The dielectric loss values were 0.01 or lower in all the samples. Permittivity values reported before for cubic/tetragonal ZrO₂ range from 20 to 40.^{29–31} However, comparison between the studies is often difficult because of the differences in film thicknesses, electrodes, thermal treatment, and preparation of the capacitors (i.e., vacuum breaks, use of clean room, etc.).

The leakage current density–electric field curves are shown in Fig. 9 for the films deposited at 300 °C by the three processes using ozone as the oxygen source. When the electrons were injected from the bottom electrode (positive electric field), the film deposited with the Zr(MeCp)(TMEA)/O₃ process had clearly higher leakage current density compared

TABLE III. Key properties for the studied ZrO₂ processes and some previously published processes for comparison.

Zr source	O source	T _{Zr} (°C)	T _{sat} (°C)	Growth rate at T _{sat} or T _{best} (Å/cycle)	C (at. %) ^a	Crystalline phase ^b	Reference
Zr(Me ₅ Cp)(TEA)	O ₃	115	300–375	0.3–0.4	<0.1–0.3	t or t + m	
	H ₂ O	—	—	0.1 (400 C)	— ^c	t	
Zr(Cp)(ⁱ BuDAD) (O ⁱ Pr)	O ₃	65	250	0.5	1.4	t or t + m	
	H ₂ O	—	—	0.43 (300 C)	2.5	t	
Zr(MeCp)(TMEA)	O ₃	120	—	0.5 (300 C)	0.8	t or t + m	
	H ₂ O	—	—	0.25 (300 C)	2.6	t (m)	
ZrCp(NMe ₂) ₃	O ₃	60	300	0.9	<1	c	20
Zr(NEtMe) ₄	O ₃	110	275	1.0	>1 (300 C)	c + m	20
ZrCp ₂ (CH ₃) ₂	O ₃	70	350	0.55	0.2	m + o	9
	H ₂ O	—	350	0.43	<0.1	m + o	21
Cp ₂ ZrCl ₂	O ₃	140	300	0.53	<0.5	m + o	9
ZrCl ₄	H ₂ O	155	500	0.50	Cl < 0.5	a (m/t)	12
Zr(thd) ₄	O ₃	170	375	0.24	<0.5	m + o	9

^aH is also a common impurity, but it was not reported for all processes.^bCrystalline phase depends on the deposition temperature and film thickness.^cNo compositional analysis was done.

to the other processes whereas from the opposite direction, there is no difference. The higher leakage current could be caused by hydrogen impurities or lower quality of the film/bottom electrode interface compared to the other processes. In the case of $\text{Zr}(\text{Cp})(^t\text{BuDAD})(\text{O}^i\text{Pr})$, clearly higher leakage current densities were obtained with water than with ozone as the oxygen source. The higher impurity content (especially carbon) and lower density of the films deposited with water compared to ozone are a likely cause for the higher leakage current density. With $\text{Zr}(\text{Me}_5\text{Cp})(\text{TMEA})$, the values were in the same range with both oxygen sources. With the $\text{Zr}(\text{Me}_5\text{Cp})(\text{TEA})/\text{O}_3$ process, leakage current densities were in the order of 10^{-8} A/cm^2 at 1 MV/cm. Very low leakage current of $2 \cdot 10^{-8} \text{ A/cm}^2$ was also measured for the $\text{Zr}(\text{Cp})(^t\text{BuDAD})(\text{O}^i\text{Pr})/\text{O}_3$ process, whereas with $\text{Zr}(\text{MeCp})(\text{TMEA})$, the leakage current densities were in the order of 10^{-7} and 10^{-6} A/cm^2 for both water and ozone deposited films. Leakage current densities for the different capacitors measured at 1 MV/cm are shown in Table II.

IV. SUMMARY AND CONCLUSIONS

Three heteroleptic Zr precursors, $\text{Zr}(\text{Me}_5\text{Cp})(\text{TEA})$, $\text{Zr}(\text{Cp})(^t\text{BuDAD})(\text{O}^i\text{Pr})$, and $\text{Zr}(\text{MeCp})(\text{TMEA})$, were studied for the ALD of ZrO_2 using water or ozone as the oxygen source. The growth rates, crystal phases, impurity contents, and electrical properties were evaluated. Excellent film purity was achieved with all the Zr precursors with ozone and especially with the $\text{Zr}(\text{Me}_5\text{Cp})(\text{TEA})$ precursor where pure ZrO_2 films were deposited with impurity levels below or at the detection limit (0.1 at. %) of TOF-ERDA. With water, higher impurity levels were detected compared to ozone, but water favored the formation of the high- κ tetragonal ZrO_2 phase. With ozone, most films were mixtures of tetragonal and monoclinic phases with the monoclinic peak intensity increasing with increasing deposition temperature. The best precursor was found to be $\text{Zr}(\text{Me}_5\text{Cp})(\text{TEA})$ with excellent thermal stability; self-limiting growth was achieved at as high as 375 °C with a growth rate of 0.4 Å/cycle. These films also had low leakage current densities in the order of 10^{-8} A/cm^2 at 1 MV/cm. Key features of the processes are collected in Table III and compared with selected processes from the literature.

ACKNOWLEDGMENTS

Funding from the Finnish Centre of Excellence in Atomic Layer Deposition (Academy of Finland) is gratefully

acknowledged. The authors thank the Electron Microscopy Unit of the Institute of Biotechnology, University of Helsinki for TEM instrument access.

- ¹D. Panda and T.-Y. Tseng, *Thin Solid Films* **531**, 1 (2013).
- ²L. Fu, Y. Li, G. Han, X. Gao, C. Chen, and P. Yuan, *Microelectron. Eng.* **172**, 26 (2017).
- ³J. H. Shim, C.-C. Chao, H. Huang, and F. B. Prinz, *Chem. Mater.* **19**, 3850 (2007).
- ⁴P.-C. Su, C.-C. Chao, J. H. Shim, R. Fasching, and F. B. Prinz, *Nano Lett.* **8**, 2289 (2008).
- ⁵M. Godlewski, S. Gieraltowska, L. Wachnicki, R. Pietuszk, B. S. Witkowski, A. Slonska, Z. Gajewski, and M. M. Godlewski, *J. Vac. Sci. Technol. A* **35**, 021508 (2017).
- ⁶J. Robertson, *J. Vac. Sci. Technol. B* **18**, 1785 (2000).
- ⁷K. Negita, *Acta Metall.* **37**, 313 (1989).
- ⁸C. L. Dezelah, J. Niinistö, K. Kukli, F. Munnik, J. Lu, M. Ritala, M. Leskelä, and L. Niinistö, *Chem. Vap. Deposition* **14**, 358 (2008).
- ⁹M. Putkonen and L. Niinistö, *J. Mater. Chem.* **11**, 3141 (2001).
- ¹⁰T. Blanquart et al., *Chem. Mater.* **25**, 3088 (2013).
- ¹¹M. Ritala and M. Leskelä, *Handbook of Thin Film Materials*, edited by H. S. Nalwa (Academic, San Diego, CA, 2002), Vol. 1, Chap. 2, pp. 103–159.
- ¹²M. Ritala and M. Leskelä, *Appl. Surf. Sci.* **75**, 333 (1994).
- ¹³S.-Y. Lee, H. Kim, P. C. McIntyre, K. C. Saraswat, and J.-S. Byun, *Appl. Phys. Lett.* **82**, 2874 (2003).
- ¹⁴M. Copel, M. Gribelyuk, and E. Gusev, *Appl. Phys. Lett.* **76**, 436 (2000).
- ¹⁵C. M. Perkins, B. B. Triplett, P. C. McIntyre, K. C. Saraswat, S. Haukka, and M. Tuominen, *Appl. Phys. Lett.* **78**, 2357 (2001).
- ¹⁶D. M. Hausmann, E. Kim, J. Becker, and R. G. Gordon, *Chem. Mater.* **14**, 4350 (2002).
- ¹⁷B. Lee et al., *Microelectron. Eng.* **86**, 272 (2009).
- ¹⁸J. Niinistö, T. Blanquart, S. Seppälä, M. Ritala, and M. Leskelä, *ECS Trans.* **64**, 221 (2014).
- ¹⁹C. Musgrave and R. Gordon, *Future Fab Int.* **18**, 126 (2005).
- ²⁰J. Niinistö et al., *J. Mater. Chem.* **18**, 5243 (2008).
- ²¹M. Putkonen, J. Niinistö, K. Kukli, T. Sajavaara, M. Karppinen, H. Yamauchi, and L. Niinistö, *Chem. Vap. Deposition* **9**, 207 (2003).
- ²²J. Niinistö, T. Hatanpää, M. Kariniemi, M. Mäntymäki, L. Costelle, K. Mizohata, K. Kukli, M. Ritala, and M. Leskelä, *Chem. Mater.* **24**, 2002 (2012).
- ²³Air Liquide press release 21 March 2013, see: <https://www.airliquide.com/united-states-america/air-liquide-electronics-strengthens-patent-portfolio-zirconium-based-high-k>, accessed 28 June 2018.
- ²⁴K. Väyrynen, T. Hatanpää, M. Mattinen, M. Heikkilä, K. Mizohata, K. Meinander, J. Räisänen, M. Ritala, and M. Leskelä, *Chem. Mater.* **30**, 3499 (2018).
- ²⁵Y. R. Luo, *Comprehensive Handbook of Chemical Bond Energies* (CRC, Boca Raton, FL, 2007, revised 2009).
- ²⁶J. Niinistö et al., *J. Mater. Chem.* **18**, 3385 (2008).
- ²⁷A. Navrotsky, *J. Mater. Chem.* **15**, 1883 (2005).
- ²⁸K. Knapas and M. Ritala, *Chem. Mater.* **20**, 5698 (2008).
- ²⁹S. K. Kim and C. S. Hwang, *Electrochem. Solid-State Lett.* **11**, G9 (2008).
- ³⁰A. Lamperti, L. Lamagna, G. Congedo, and S. Spiga, *J. Electrochem. Soc.* **158**, G221 (2011).
- ³¹I. Kärkkäinen, A. Shkabko, M. Heikkilä, J. Niinistö, M. Ritala, M. Leskelä, S. Hoffmann-Eifert, and R. Waser, *Phys. Status Solidi A* **211**, 301 (2014).